Materials & Design 185 (2020) 108251

Contents lists available at ScienceDirect

Materials & Design

journal homepage: www.elsevier.com/locate/matdes

Improved fracture toughness by microalloying of Fe in Ti-6Al-4V

Fuwen Chen [a], Yulei Gu [a], Guanglong Xu [a, *], Yuwen Cui [a, b], Hui Chang [a], Lian Zhou [a]

[a] Tech Institute for Advanced Materials & College of Materials Science and Engineering, Nanjing Tech University, Nanjing, 210009, China
[b] Instituto de Ciencia de Materiales de Aragon (ICMA), Zaragoza, 50009, Spain

HIGHLIGHTS

- The microalloying of Fe in Ti−6Al−4V can effectively improve the fracture toughness.
- The Fe-alloyed Ti−6Al−4V shows comparable mechanical properties to TC4ELI and TC4DT.
- The interaction between Fe and V leads to enhanced modulus and increases fracture toughness of TC4F.
- The kinked β+α lamellae are found nearby the crack of TC4F in contrast with bent α lamellae in TC4.

GRAPHICAL ABSTRACT

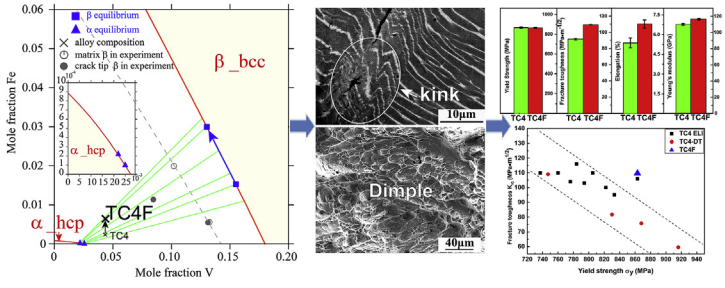

ARTICLE INFO

Article history:
Received 7 July 2019
Received in revised form
23 September 2019
Accepted 2 October 2019
Available online 4 October 2019

Keywords:
Micro-alloying of Fe
Ti−6Al−4V
Fracture toughness
Enhanced modulus
Composition redistribution of V and Fe

ABSTRACT

The widely used Ti−6Al−4V (TC4) titanium alloy has been modified through the micro-alloying of Fe. The microstructural features and mechanical properties of the designed alloy, TC4F, are compared with other alloys in Ti−6Al−4V class by combining experimental characterizations and thermodynamic calculations. TC4F alloy not only maintains strength, hardness, and elongation similar to baseline TC4 but also exhibits improved fracture toughness comparable to TC4_ELI and even superior to TC4_DT under the heat-treated condition. It opens up a new cost-reducing way to enhance fracture toughness in place of controlling interstitial contents, showing potential in engineering applications. The discerned mechanisms indicate that the trace addition of Fe gives rise to composition redistribution between V and Fe in the β phase, boosts the lattice distortion and vibration, thereafter enhances Young's modulus and fracture toughness. It has been validated and verified by experiments, thermodynamic calculations, and Hahn-Rosenfield empirical research. The enhanced fracture toughness also benefits from the kinked β+α lamellar microstructure at crack tip as well as the improved fracture surface due to the Fe addition. The enlarged plastic zone, redirected crack propagation, and more dimples with even-distributed size additionally contribute to the improvement of fracture toughness.

1. Introduction

Ti−6Al−4V alloy was firstly developed in 1954 [1] and has been the workhorse in the titanium industry. It provides superior specific strength and corrosion resistance to aluminum alloys and low alloy steels [2]. The forgiving nature of thermomechanical processing renders the wide usage of this alloy on aircraft, covering landing gear beam, windshield frames, fin deck attached to the fuselage, etc. [3] It thus has accounted for more than 60% of total titanium products in aircraft industry [4].

Over the past half century, great efforts have been put to upgrade the performance of Ti−6Al−4V by uing different strategies. These strategies cover multicomponent alloying in composition

* Corresponding author.
E-mail address: guanglongxu@njtech.edu.cn (G. Xu).

https://doi.org/10.1016/j.matdes.2019.108251

design, advances in melting (e.g. electron beam melting [5,6], selective laser melting [6,7]), novel powder metallurgy (e.g. selective laser sintering [7]) and sophisticated deformation techniques (e.g. isothermal forging [8] and ultrasonic surface rolling [9]). Among these techniques, multicomponent alloying has been proved to be a simple and effective way. The primary task of the alloying was to improve strength. Many follow-ups alloys, such as Ti−6Al−6V−2Sn [10] and Ti−6Al−2Sn−4Zr−6Mo [11], have been viewed as higher strength versions of Ti−6Al−4V. Fe is much cheaper than other alloying elements but provides a strong effect of β stabilization. It has served as a macro-alloying element. Ti−6Al−1.2Fe was designed as a low-cost alternative to Ti−6Al−4V with comparable strength at ambient temperature. The smaller amount of Fe was selected based on the equivalence of β stability between Fe and V. Ti-155A(Ti−5Al−1.5Fe−1.4Cr-1.2Mo) exhibited higher yield and ultimate strengths in tension but lower crack resistance in forging than Ti−6Al−4V [12]. Even a simple Ti−3Fe alloy can obtain a high strength of 1300 MPa readily via heat treatment [13]. Therefore, the Fe element has a distinctive performance in solid solution strengthening and cost saving.

The improved working properties also benefit from the addition of Fe [14]. The refinement of β grain size has been found in Ti−6Al−4V modified by 0.1−1.0 wt% Fe [15], and thus facilitated the subsequent forging. The effect of Fe alloying also has been realized in the decreased forming temperature and increased forming rates. SP-700(Ti−4.5Al−3V−2Mo-2Fe) was designed to offer excellent hot forgeability, cold formability and heat treatability superior to Ti−6Al−4V [16].

More than high strength and workability, the alloy design concept of damage tolerance has been more and more widely accepted [17]. It requires that titanium components have the ability to sustain defects safely until a repair can be effected. The plane strain fracture toughness (K_{IC}) is one of important damage tolerance properties. It depicts the resistance to unstable crack propagation. The alloys with high K_{IC} promote crack blunting and plastic energy dissipation before the crack tips. There are two ways to improve the fracture toughness of Ti−6Al−4V. (1) Microstructure tailoring through optimizing processing parameters. For example, BASCA heat treatment can provide α/β lamellar microstructure with the highest fracture toughness. It is implemented by a solid solution in the β phase region followed by furnace cooling to the target temperature in the α+β phase region, and then annealing at the final temperature [18]. The maximum fracture toughness K_{IC} reaches 90 MPa $m^{1/2}$ [19]. However, the enhanced fracture toughness is obtained at the expense of strength reduction. (2) Modifying Ti−6Al−4V through alloying. Ti−6Al−4V ELI (extra low interstitials) grade alloy provides improved fracture toughness comparing to grade 5 Ti−6Al−4V alloy [20]. It has low contents of $O \leq 0.13$ and $Fe \leq 0.25$ [21]. The K_{IC} of heat treated Ti−6Al−4V ELI is optimized to 110 MPa $m^{1/2}$ [22]. Ti−6Al−4V DT has been designed via mediating O content between ELI and commercial grades [23], showing a maximum oxygen content of 0.12 wt % against 0.20 wt % in commercial grade Ti−6Al−4V. It combines moderate strength, high toughness and low crack propagating rate. The maximum fracture toughness of Ti−6Al−4V DT is around 100 MPa $m^{1/2}$ in Ref. [23].

Preliminary investigations by the present authors and other researchers indicate that the addition of 0.55 wt% Fe to Ti−6Al−4V reduces the high-temperature flow stress and improves hot workability [24] and might be expected to improve comprehensive mechanical properties including fracture toughness [25]. In present work, Ti−6Al−4V alloys with and without 0.55 wt% Fe micro-alloying are prepared under the same processing conditions. The changes of microstructural characteristics, mechanical properties and crack behaviors due to the minor addition of Fe are scrutinized through comparisons between two alloys. In particular, the effect of Fe addition on the fracture toughness of Ti−6Al−4V and the underlying mechanisms behind the experimental phenomena are attempted to figure out.

2. Experimental procedures and methodology of data analyses

2.1. Materials

The Ti−6Al−4V alloys with and without micro-alloying of Fe in the present experiments were provided by BAOTI group Co., Ltd. The as-received plates with a thickness of 14 mm were produced by Vacuum Arc Remelting (VAR) followed by hot rolling in β and α+β regions. The processing parameters in VAR and hot rolling were controlled same for both alloys. The PS-6 inductively coupled plasma was employed to detect the chemical compositions of the alloys. The actual compositions of Al and V are almost identical to those of nominal compositions. Only the composition difference in Fe is noticeable between the two alloys (Table 1). Note that the composition differences of other elements are negligible because their differences show one order of magnitude smaller than that of Fe. The fabricated alloys are thus qualified in chemical composition to study the effect of micro-alloying of Fe in Ti−6Al−4V.

2.2. Heat treatment

The β-transus temperatures of Ti−6Al−4V alloys with and without Fe micro-alloying were determined respectively as 975 ± 5 and 965 ± 5 °C by the metallographic method. A BASCA heat treatment was subsequently designed based on the determined β-transus temperatures. It consisted of a solid solution at 1100 °C for 40 min, furnace cooling to 712 °C, 2 h annealing at 712 °C, and air cooling. The heat-treated Ti−6Al−4V and Fe micro-alloyed Ti−6Al−4V alloys (hereinafter referred to as "TC4" and "TC4F") would exhibit β+α lamellar microstructure which is generally favorable for fracture toughness. With the BASCA heat treatment, the preceding microstructure formed in arc melting and hot rolling had been eliminated to the most extent as well as the inhomogeneous distribution of residual stress/strain. The heat-treated microstructure of β+α lamellae ensures that the microstructure distinctions and the difference in mechanical properties between TC4 and TC4F alloys in the following characterizations would be furthest attributed to the thermodynamic nature of Fe alloying.

2.3. Mechanical property test

Room temperature tension, mode-I fracture toughness and Vickers hardness (H_V) were carried out to evaluate the mechanical properties of TC4 and TC4F alloys. The tensile test was performed on an INSTRON-5581 with a rate of 0.02 mm/s. Cylindrical tensile specimens were wire cut from heat-treated plates with the tensile direction parallelling to the rolling direction. The shape and dimension of the specimen for tension at room temperature are illustrated in Fig. 1(a) The gauge length was set 100 mm and the gauge diameter was set 10 mm according to ASTM E 8M – 04 [26].

Table 1
Chemical compositions of Ti-6Al-4V and Fe microalloying Ti-6Al-4V alloys.

Alloy	Al	V	Fe	C	N	O	H	Si
TC4	6.21	4.20	0.200	0.010	0.010	0.17	0.001	0.015
TC4F	6.20	4.14	0.537	0.020	0.020	0.13	0.001	0.016
Deviation	−0.01	−0.06	+0.337	+0.010	+0.010	−0.04	0	+0.0001

The tensile tests were conducted three times for each alloy to avoid anomalous measurements. Ultimate tensile strength (σ_s), yield tensile strength (σ_y), elongation (δ %), elastic modulus (E), and strain hardening exponent (n) were obtained averaging over measurements applicable.

Mode-I fracture toughness in the condition of plane strain, K_{IC}, was performed on an INSTRON-651 with an electro-hydraulic servo system. The chevron-notched half compact-tension specimens were wire cut with L–T (rolling–long transverse) orientations from the plates and machined as per ASTM standard E399-06 [27]. The opening direction of the mode-I pre-crack was selected parallelling to the long transverse direction, and the direction of crack propagation was parallelling to the rolling direction. The dimensions of the compact tension specimen were listed as follows: thickness B = 12 mm; width W = 48 mm; notch length a_0 = 21 mm; pin center from the crack plane 13.2 mm; COD half gage length 2.5 mm; and COD distance from load line 12 mm. The 24 mm pre-cracks were preset at a constant ΔK of 21 MPa $m^{1/2}$ with a sinusoidal waveform at a frequency of 10 Hz. The fracture toughness was calculated using the formula given in the ASTM standard E399, and the final value of mode-I fracture toughness was obtained by averaging the testing values of four measurements. The schematic drawing of the compact-tension specimen for fracture toughness test is illustrated in Fig. 1((b).

The Vickers hardness measurement was performed on an HV-1000 testing machine using an indentation load of 200 kg for a dwell time of 10s. The hardness values were averaged over 50 different locations in each alloy.

2.4. Microstructure characterization

FEI Quanta Scanning Electron Microscope (SEM) was used to observe the microstructure before and after fracture toughness test. With the SEM images, the phase size and the phase fraction were obtained by using Image-Pro Plus software. It is noteworthy that the phase size and the phase fraction were repetitively measured in different areas, thus the mean values are of statistical significance. The local chemical compositions of phases were detected by an Electron Probe Micro-Analyzer (EPMA, JEOL JXA 8900). Electron Back-Scattered Diffraction(EBSD) measurement was conducted on a ZEISS Sigma 500 at an accelerating voltage of 20 kV with a step size of ~1 μm. Surface preparation for EPMA, SEM, and EBSD consisted of grinding on successively finer SiC paper, manual polishing with 0.5 μm diamond paste, and finally, chemo-mechanical polishing using a solution of colloidal silica. The phase constitutions were detected on the Rigaku Ultima IV X-Ray Diffractometer(XRD) using Cu Kα radiation (λ = 1.5406 Å). It was operated at 40 kV, 40 mA with the scanning rate of 1°/min and 2θ range of 30–80°.

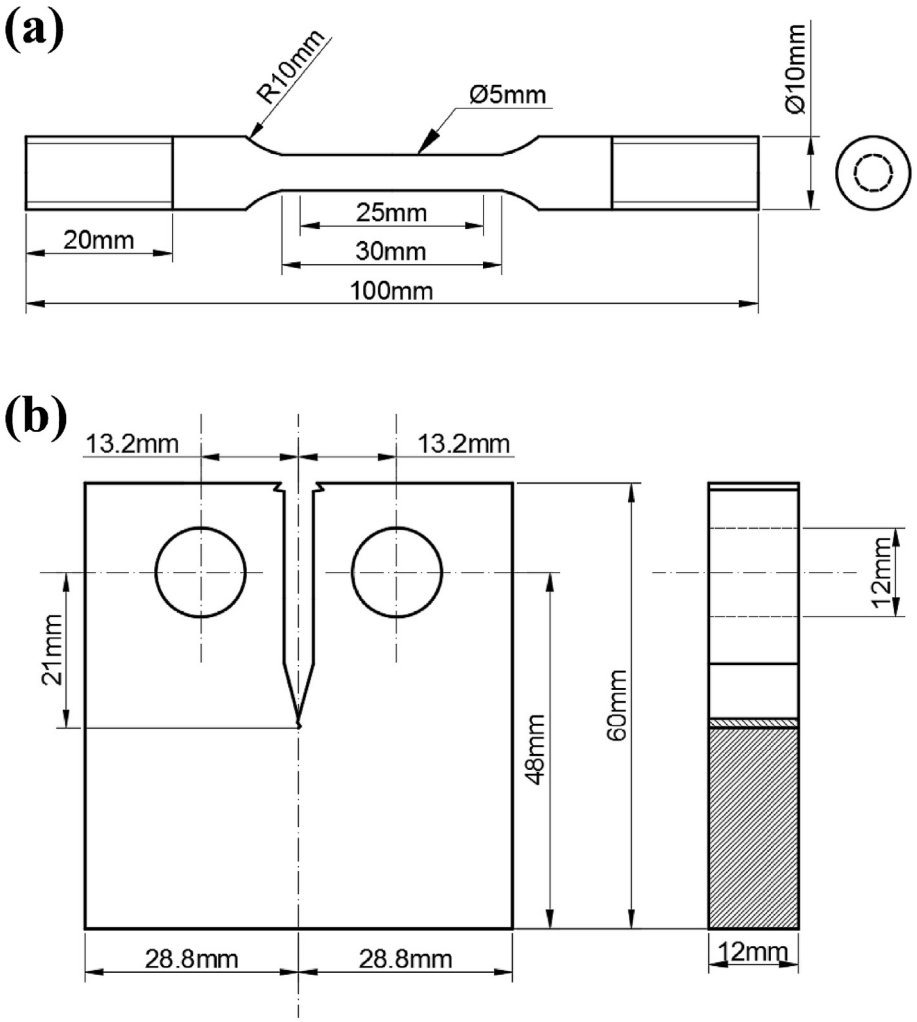

Fig. 1. Shape and dimension of (a) the specimen for tension at room temperature, (b) the compact-tension specimen for fracture toughness test.

The state of the residual stress on the specimens was measured following [9]. It was carried out on an LXRD laboratory residual stress measurement system with the Cu Kα radiation, irradiated area 3.14 mm^2, and Bragg angle 142°. The $sin^2\Psi$ method was implemented to estimate the residual stress. The residual stress distribution with depths was conducted after successive layer removal using electrochemical polishing with NaCl solution.

3. Results and discussions

3.1. Mechanical properties in macroscale

Fig. 2 compares the mechanical properties of TC4 and TC4F examed in present work. The statistical average values of the measurements are summarized in Table 2. The yield tensile strength (σ_y) hardly changes with the micro-alloying of Fe, showing values of 866.47 MPa in TC4 *versus*. 864.17 MPa in TC4F. The ultimate tensile strength (σ_s) decreases slightly with the addition of Fe, from 896.07 MPa in TC4 to 878 MPa in TC4F. The elongation (δ%), mode-I fracture toughness (K_{IC}), Young's modulus (E), and Vickers hardness (H_V) increase at different levels with the addition of Fe. The improved ductility is limited, manifested by the slightly increased δ% from 5.33% of TC4 to 6.77% of TC4F. Both measured elongations around 6% fall within ranges considered normal, despite the misguided percentage of 27.12% for the improvement. The improvements of E and H_V are moderate, showing comparable percentages of 5.83% and 5.78%, respectively. The tested Young's modulus of 110 GPa for TC4 is close to that in Ref. [28] under a similar tensile condition after heat treatment. The most remarkable of all mechanical properties is the fracture toughness, K_{IC}. The trace addition of Fe is capable of boosting the performance of fracture toughness in TC4. K_{IC} has been measured 109.48 MPa $m^{1/2}$ in TC4F in comparison with 91.45 MPa $m^{1/2}$ in TC4 baseline alloy.

Fig. 3 compares the combinatorial performance of σ_y and K_{IC} among TC4F, Ti−6Al−4V_ELI, and Ti−6Al−4V_DT which all belong to the class of modified Ti−6Al−4V. The combinatorial performance of σ_y and K_{IC} examined in TC4F is obviously superior to that of Ti−6Al−4V_DT in Ref. [23] and slightly above the optimum performance of Ti−6Al−4V_ELI in Ref. [22]. As is mentioned in the previous section, Ti−6Al−4V_ELI and Ti−6Al−4V_DT are damage tolerance alloys modified from original Ti−6Al−4V. Despite the good performance of fracture toughness, the preparation of Ti−6Al−4V_ELI or Ti−6Al−4V_DT requires precise control of the contents of interstitial elements via finding a balance between the addition of TiO_2 and volatilization of interstitial elements in VAR, thus gives rise to a higher cost than commercial Ti−6Al−4V alloy. Based on the discovery of present work, the microalloying of Fe opens a new way to improve fracture toughness in a cost-reducing manner without additional control of interstitial elements.

3.2. Phase and crack morphology

To figure out the physical metallurgical reasons for the improved fracture toughness, the microstructure observation has been carried out. Fig. 4 (a) and (b) show SEM back-scattered electron images of the microstructure of TC4 and TC4F in the heat-treated state before the fracture toughness test. The images illustrate the phase contrast of α in grey and β in white. The two alloys show the similar β+α lamellar microstructure with alternate layers of α and thin β. Most of the α lamellae are oriented along preferred orientations to form colonies. Whereas, some colonies are randomly placed, showing deviations from the preferred orientation. The addition of Fe slightly changes amount and size of phases. The α phase in TC4F has been apt to form narrower lamellae and decrease in volume fraction. The β layers are correspondingly increased in width and phase fraction. The variations of phase fraction and width are

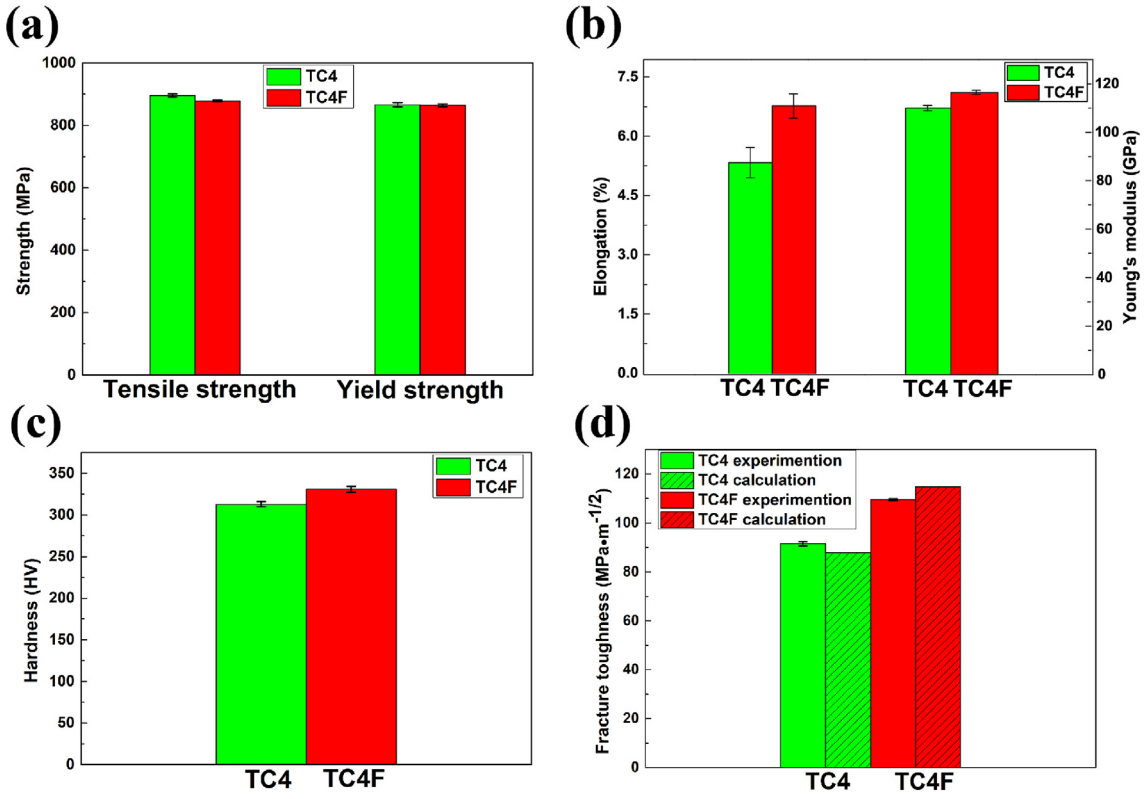

Fig. 2. Mechanical properties of TC4 and TC4F: (a) tensile strength and yield strength, (b) elongation and Young's modulus (c) Vickers hardness, and (d) fracture toughness.

Table 2
Mechanical properties of TC4 and TC4F alloys.

Alloy	Tensile properties					Hardness (H_V)	Experimented fracture toughness K_{IC} (MPa $m^{1/2}$)	Calculated fracture toughness K_{IC} (MPa $m^{1/2}$)
	Tensile strength σ_s (MPa)	Yield strength σ_y (MPa)	Elongation δ (%)	Young's modulus E (GPa)	n			
TC4	896.07 ± 4.36	866.47 ± 6.59	5.33 ± 0.38	110.00 ± 1.08	0.135	312.87 ± 3.16	91.45 ± 0.88	87.93
TC4F	878.00 ± 2.69	864.17 ± 4.43	6.77 ± 0.31	116.42 ± 0.88	0.152	330.96 ± 3.49	109.48 ± 0.34	114.81
Difference	−2.01%	−0.27%	+27.12%	+5.83%	+12.59%	+5.78%	+19.72%	

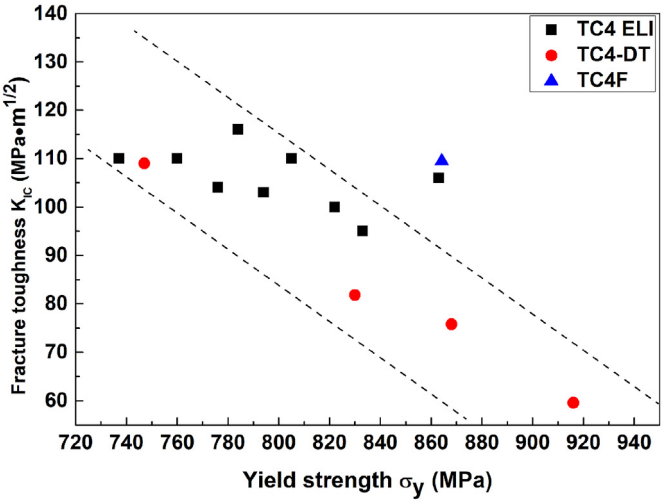

Fig. 3. σ_y-K_{IC} comparison among TC4F, TC4-DT and TC4 ELI (TC4 ELI [23], TC4-DT [22]).

visualized in Fig. 5, and the statistical average values of these morphology parameters are listed in Table 3. To verify the results of SEM observation, Fig. 6 shows the XRD patterns of TC4 and TC4F in the same heat-treated state. The phase constitution of (α+β) dual phases is clearly demonstrated in both alloys. The relative phase percentages derived from XRD measurement are generally in agreement with the results from SEM observation, see Fig. 6(b). In common sense, the increasing α colony/lamella size always promotes the toughness of β+α lamellar titanium alloys because the cracks are less liable to initiate at and propagate from broad lamellae [29,30]. However, the interpretation may not apply to TC4F due to the slenderer α lamellae in Fig. 4. We believe that the effects of phase size and phase fraction on fracture toughness are trivial in TC4F. If these effects had been adhered to, it can only be attributed to the formation of 'soft' β phase a little bit more in TC4F than in TC4.

Fig. 7 (a) and (b) present the morphology of the cracks in TC4 and TC4F, respectively, and the enlarged lamellar microstructure close to the crack. The SEM back-scattered electron images were

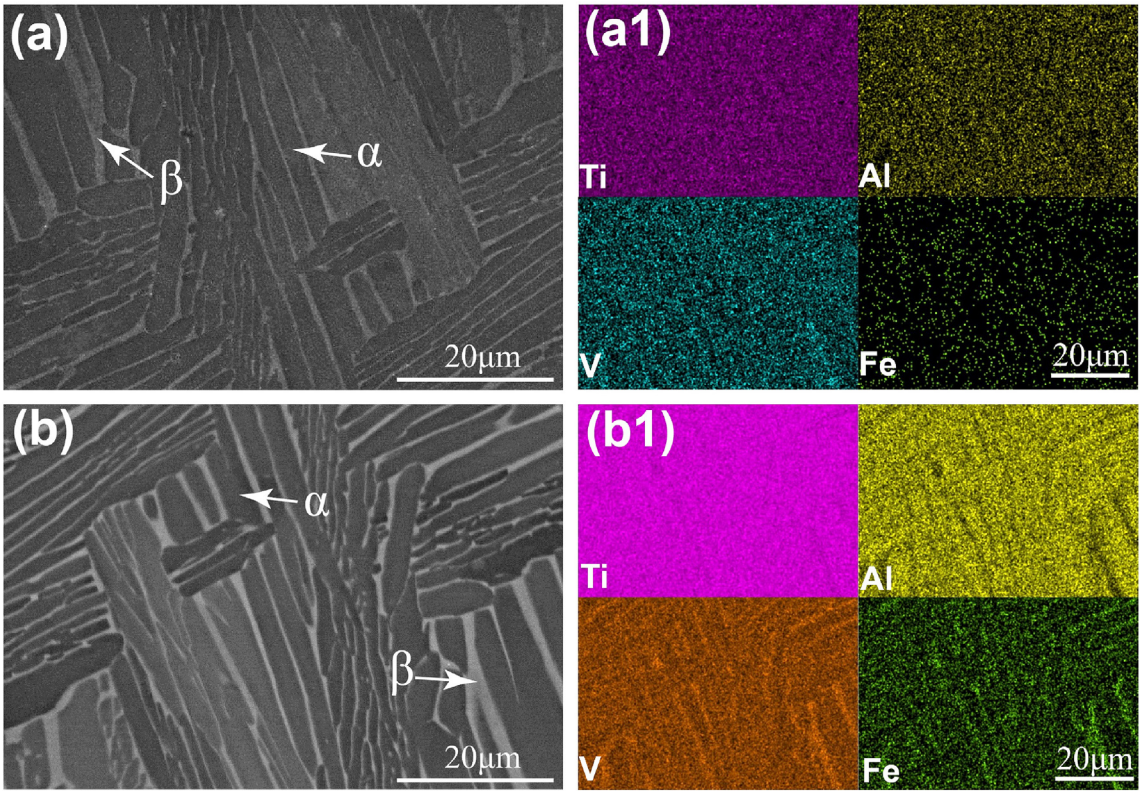

Fig. 4. SEM back-scattered electron images of the β+α lamellar microstructure in heat-treated (a) TC4 and (b) TC4F; The element distributions corresponding to the same areas in (a1) TC4 and (b1) TC4F.

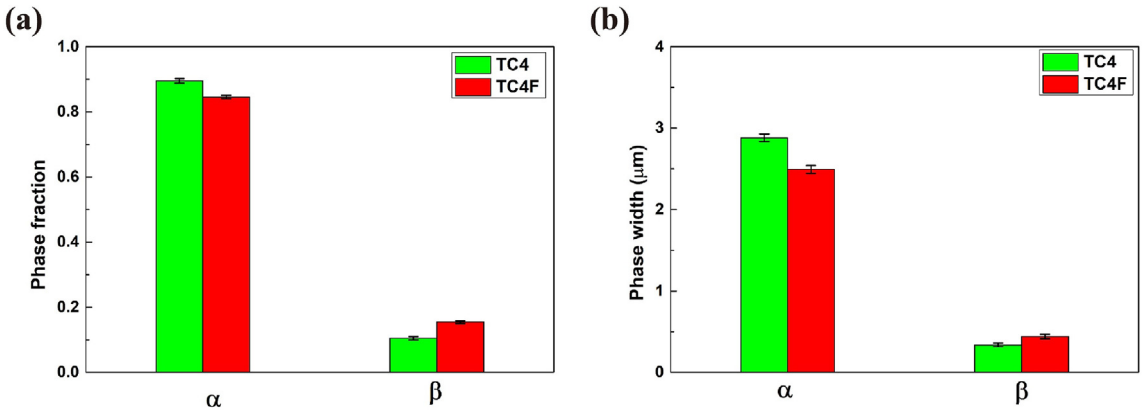

Fig. 5. The comparison of (a) phase fraction and (b) average lamella width between TC4 and TC4F.

Table 3
Microstructure features of TC4 and TC4F alloys.

Alloy	Phase percentages (vol%) by SEM		Phase percentages (vol%) by XRD		Width (μm)	
	α	β	α	β	α	β
TC4	89.54 ± 0.70	10.46 ± 0.50	90.6 ± 1.5	9.4 ± 0.3	2.881 ± 0.047	0.337 ± 0.023
TC4F	84.57 ± 0.52	15.43 ± 0.42	83.1 ± 1.8	16.9 ± 0.9	2.495 ± 0.048	0.440 ± 028
Difference	−4.97	+4.97	−7.5	+7.5	−0.386	+0.103

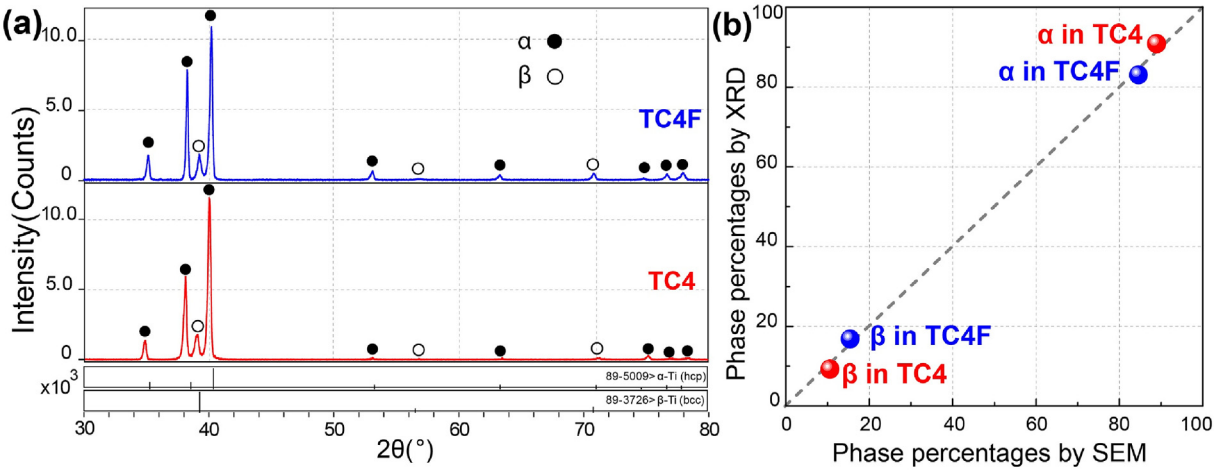

Fig. 6. (a) XRD patterns of TC4 and TC4F, (b) comparison of phase percentages obtained from XRD and SEM.

captured after fracture toughness tests. The cracks can propagate along boundaries between α colonies or layers between α/β lamellae, or even across the α colony. The change of propagation direction gives rise to the crack branching and secondary cracking. In detail, the crack prefers to propagate along the boundaries of α colonies when the direction of crack propagation is approximately parallelling to colony orientation. Otherwise, the crack has to advance along α/β interface between lamellae or even to sunder the α colony/lamellae. It is because that sundering the α colony/lamellae requires more additional energy than fracture along the colony boundaries. In TC4F, the kink of α lamellae are found in the area neighboring the crack when it crosses the α colony. However, the α phase nearby the crack of TC4 only shows a slight bent without the zigzag distortion. The formation of zigzag or river-like β+α lamellae indicates that severe plasticity deformation takes place in this region. The large plastic zone enables dissipation or absorption of accumulated energy ahead of the crack tips, slows down the rate of crack propagation, and results in increased fracture toughness of TC4F. Moreover, the kinked α lamella is oriented deviating from the preferential orientation. It helps crack change the propagation direction, thus consumes additional energy and results in increased fracture toughness. Therefore, the kinked α lamella formed in TC4F has a positive effect on the improved fracture toughness. The discussed propagation behaviors of the cracks in TC4 and TC4F are illustrated in Fig. 8.

3.3. Fractography

The fracture surfaces have been carefully examined with SEM and are shown in Fig. 9. The alloys with and without micro-alloying of Fe both display the mixed mode of fracture. Fine dimples, cleavage facets with river marking, ravines, and micropores are

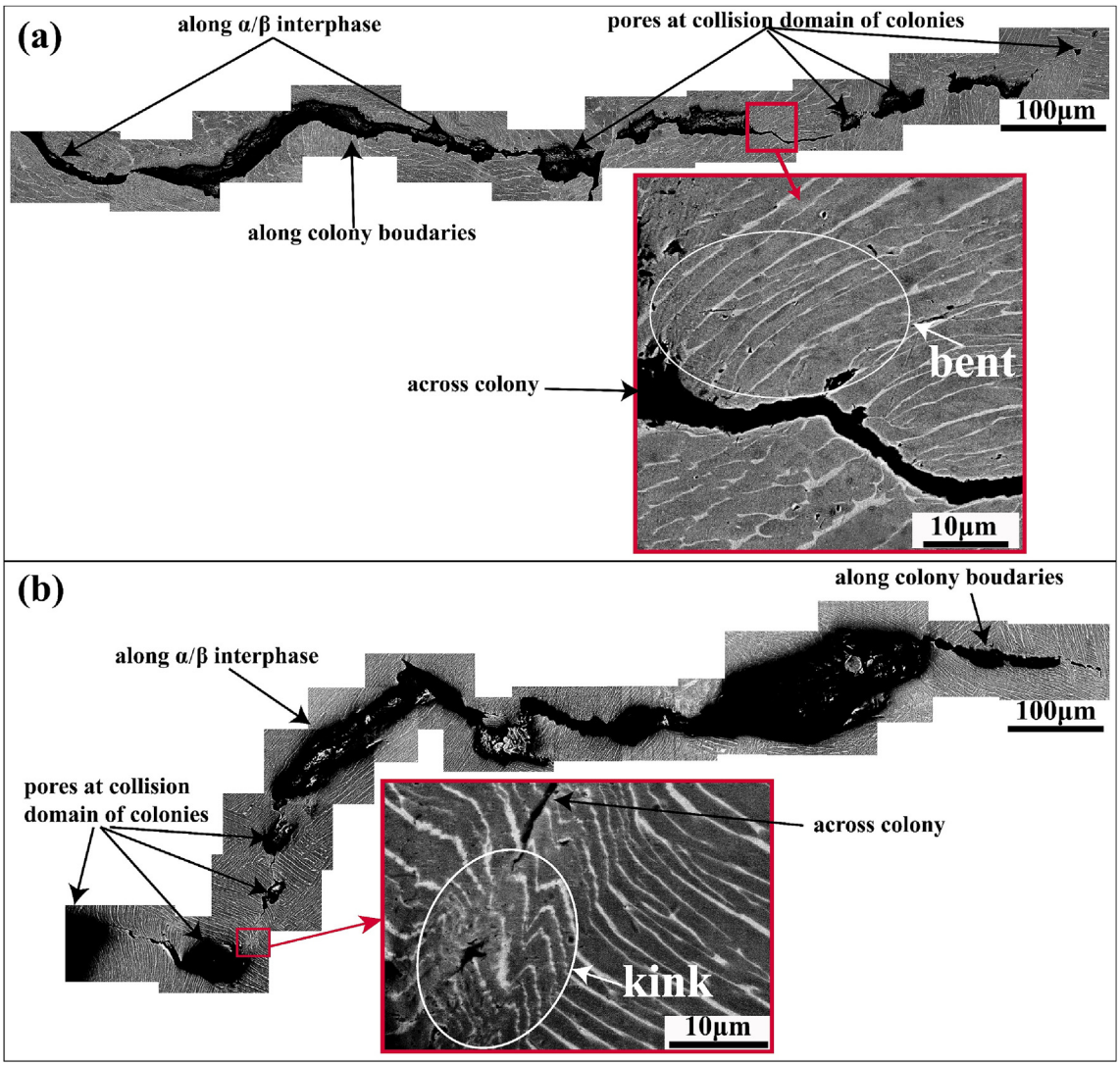

Fig. 7. SEM back-scattered electron images of crack propagation in (a) TC4 and (b) TC4F together with the enlarged microstructure close to crack.

found on the fracture surfaces. The dimple fracture is always accompanied by the formation of secondary cracking. In comparison with two alloys, the fracture surfaces of TC4F contain a larger area of dimples and a smaller area of cleavage facets than TC4. TC4F has bigger sized and even distribution of dimples, in contrast with the smaller size, fibrous and elongated dimples in TC4. Since the high fracture toughness is always associated with great numbers of dimples with relatively large size, higher undulation depth, and uniform size distribution, therefore TC4F is naturally indicating an improved fracture toughness.

3.4. Residual stress and microhardness near the fracture surface

Residual stresses have been considered as a possible toughening mechanism. It might be closely related to crack deflection, branching, bending, kink, etc. Therefore, the variations in residual stress and microhardness distribution along the depth axis perpendicular to the crack propagation are compared between TC4 and TC4F and shown in Fig. 10. The residual stresses are found to be compressive at the fracture surface and have a minimum value at a depth of about 75 μm below the surface. After that, the magnitude of the residual stresses increases with increase in depth of cut. The variation tendency is similar to that in IMI-834 [31] and the ultrasonic surface rolled TC4 [9]. With the addition of Fe, the compressive residual stresses in TC4F are more negative near the fracture surface than that in TC4, while the tensile residual stresses in TC4F are less positive in the area slightly away from the fracture than that in TC4. An increasing compressive residual stress developed in TC4F may account for the higher resistance to crack propagation and higher tendency toward crack deflection, and thus for the enhancement of fracture toughness.

The results of microhardness test indicate that the fracture surface is an area of weakest comprehensive mechanical performance. The microhardness shows relatively small value at the fracture surface and then gradually increases towards the deeper region away from the fracture surface. The variation tendency applies to both TC4 and TC4F alloys. The measured microhardness of TC4F is comparable in magnitude to that of TC4.

3.5. Misorientation mapping for visualization of local deformation

Since the non-uniform local misorientation in microstructure can be caused by the inhomogeneous deformation and thereafter influence fracture toughness, EBSD has been employed to mapping

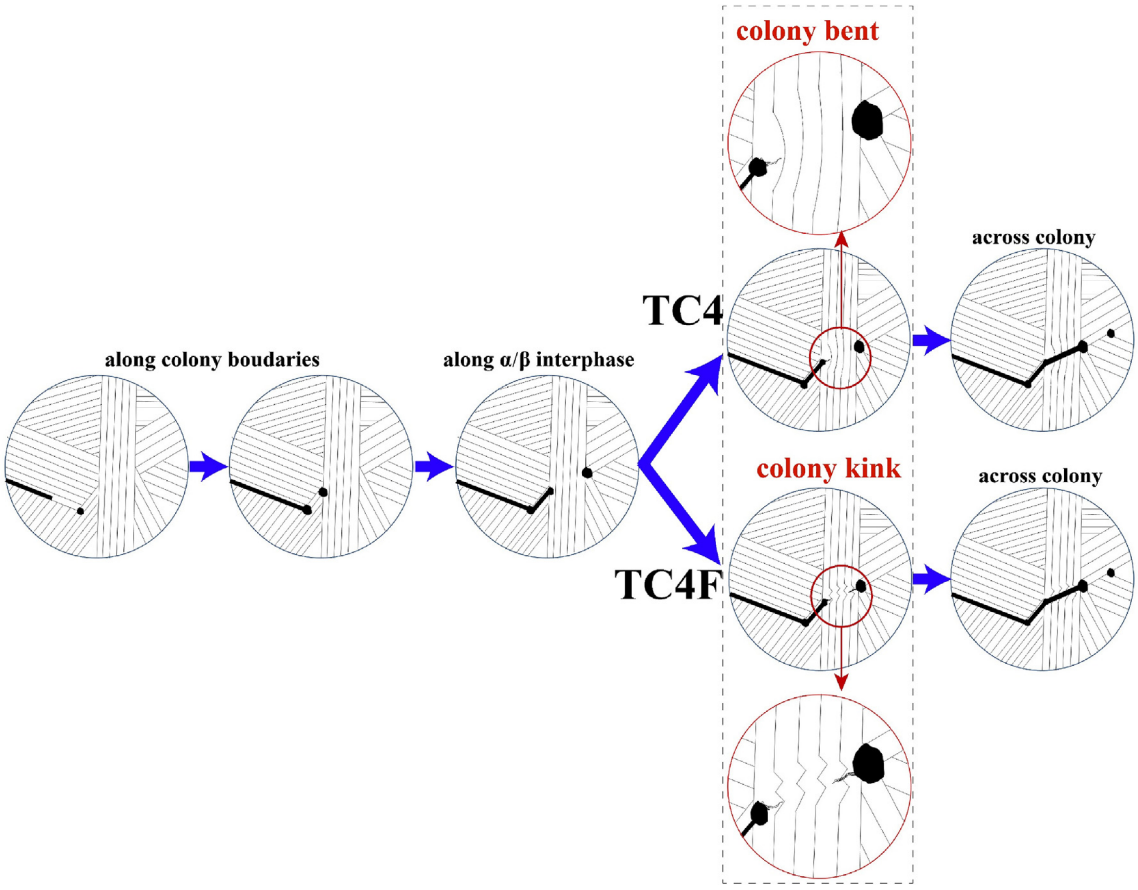

Fig. 8. The schematic drawing of crack propagation in TC4 and TC4F.

the intragrain misorientation in TC4 and TC4F which is capable of evaluating retained plastic deformation in the heat-treated β+α lamellar microstructure. The developed algorithm of average internal misorientation [32] was based on recording the internal rotation within a given grain due to plastic deformation and projecting all of these "single grain maps" onto the same microstructural visualization [33]. Fig. 11 (a) and (b) present Euler angle maps of TC4 and TC4F, showing the α colonies and the inter-lamellar β in the areas far away from the crack tip. The α colonies with several different orientations are indicated by different colors in the Euler angle map, and the α lamellae in the same colony present similar orientation. However, the Euler angle map shows no information sensitive to the retained deformation associated with the preceding smelting and rolling. Fig. 11 (a1) and (b1) show the direct mapping of the intragrain misorientation. Within each colony/lamella, the misorientation between the reference pixel and every other pixel was plotted using a color map from 0° in blue to 5° in red. Most areas in TC4 and TC4F have a blue color with small local misorientations (<0.25°) indicating small amounts of lattice rotation and/or little retained deformation in alloys. The β phase in misorientation map has a green color representing local misorientations between 0.25° and 1.5°. The black areas are mainly distributed at the α/β phase boundary. The relative larger misorientations and retained deformation are originating from the defects at the α/β interface. Demonstrated by the misorientation mapping, we conclude that the BASCA heat treatment has erased the retained strain/distortion in rolled TC4 and TC4F. Both alloys with β+α lamellar microstructure have recovered to an undeformed state. This observation allows us to infer that all the changes in microstructure and mechanical properties when TC4F is compared to TC4 in this work could be attributed to the thermodynamic nature of Fe alloying.

3.6. Composition redistribution

The overall composition distributions of TC4 and TC4F were detected by EDX and provided in Fig. 4. The partitioning behaviors of Al and β stabilizers are verified that Al preferentially partitions to the α phase, whereas V and Fe dwell in the β phase. The chemical compositions of α and β phases detected by EPMA were subjected to a crosswise comparison, i.e. w/o Fe addition (TC4F *versus*. TC4) and matrix *versus*. crack tip. The data are summarized in Table 4 together with histograms illustrated in Fig. 12. The compositions of α in TC4 are almost identical to those in TC4F, both in the matrix and near the crack tip. It indicates that the microalloying of Fe has little effect on the chemical composition of α phase. However, noticeable variations of chemical compositions take place in the β phase due to the trace addition of Fe. The chemical composition of β phase was detected Ti−4.86Al−13.27V−0.56Fe (at. %) in TC4 matrix away from the crack, in comparison with Ti−6.07Al−8.48V−1.14Fe (at. %) at a similar position of TC4F. The addition of trace Fe leads to a composition redistribution in the β phase, especially for the interaction/competition between V and Fe.

To validate the experiment results, a thermodynamic calculation was implemented using Thermo-Calc software and the TTTi3 database. The elemental contents of Ti, Al, V, Fe, O in TC4 and TC4F were considered as inputs (see Table 1). However, C, N, H, and Si were neglected because the contents of them were one order of

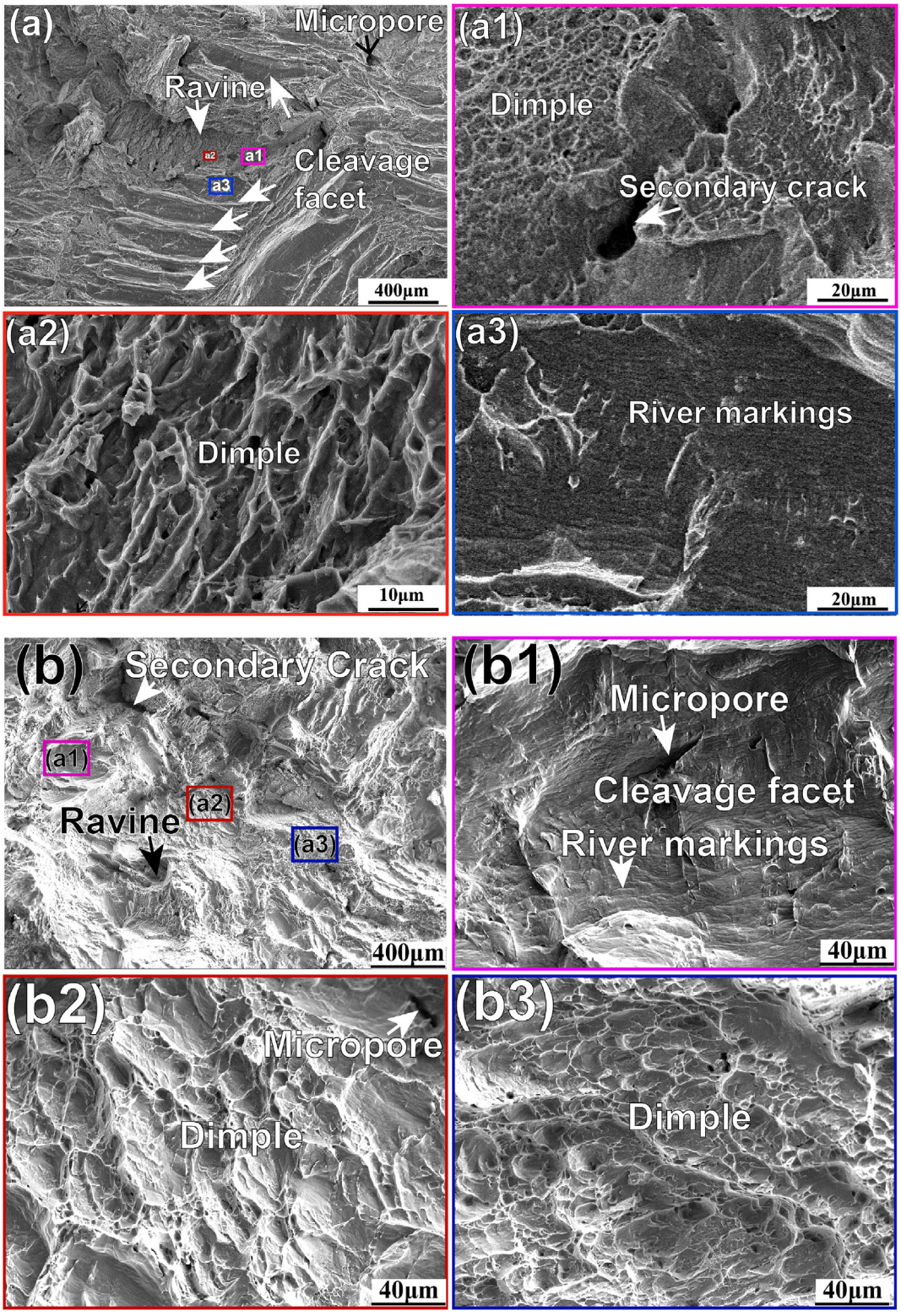

Fig. 9. Fracture surfaces of (a-a3) TC4 and (b-b3) TC4F alloys after mode-I fracture toughness test.

magnitude smaller than the formers. The β-transus temperatures were calculated 972.39 °C for TC4 and 954.07 °C for TC4F, respectively. The temperatures were close to those measured by metallographic observation, indicating the reliability TTTi3 database. The isothermal phase diagram section at 712 °C is shown in Fig. 13, which depicts the changes of α and β phases boundaries with the mole fractions of V and Fe. The redistribution behaviors discovered in experiments are well reproduced by thermodynamic calculation qualitatively. In Fig. 13, the alloy compositions of TC4 and TC4F are marked in black crosses, and the equilibrium chemical

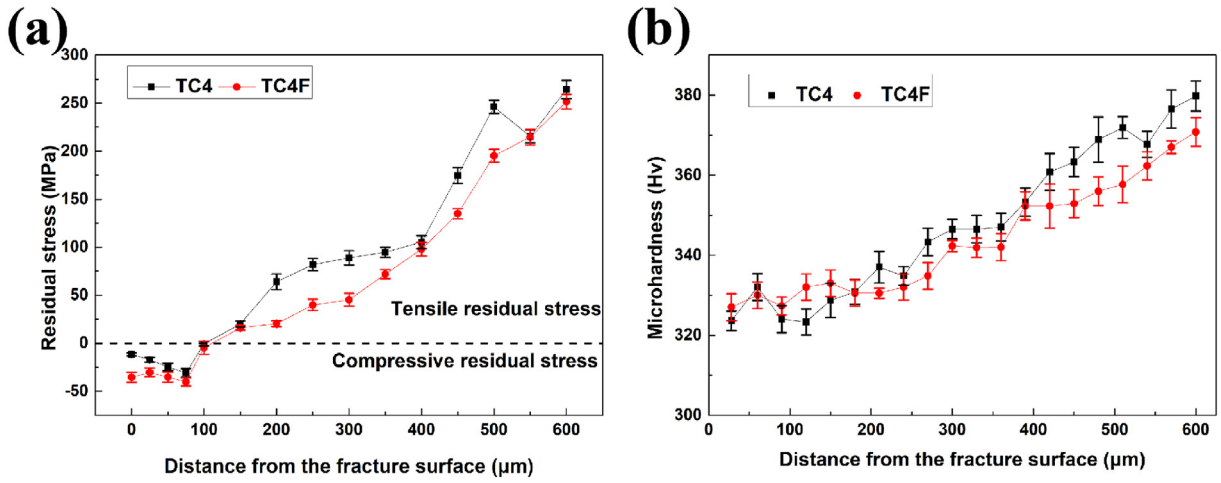

Fig. 10. Comparisons of (a) residual stress distribution and (b) microhardness variation between TC4 and TC4F.

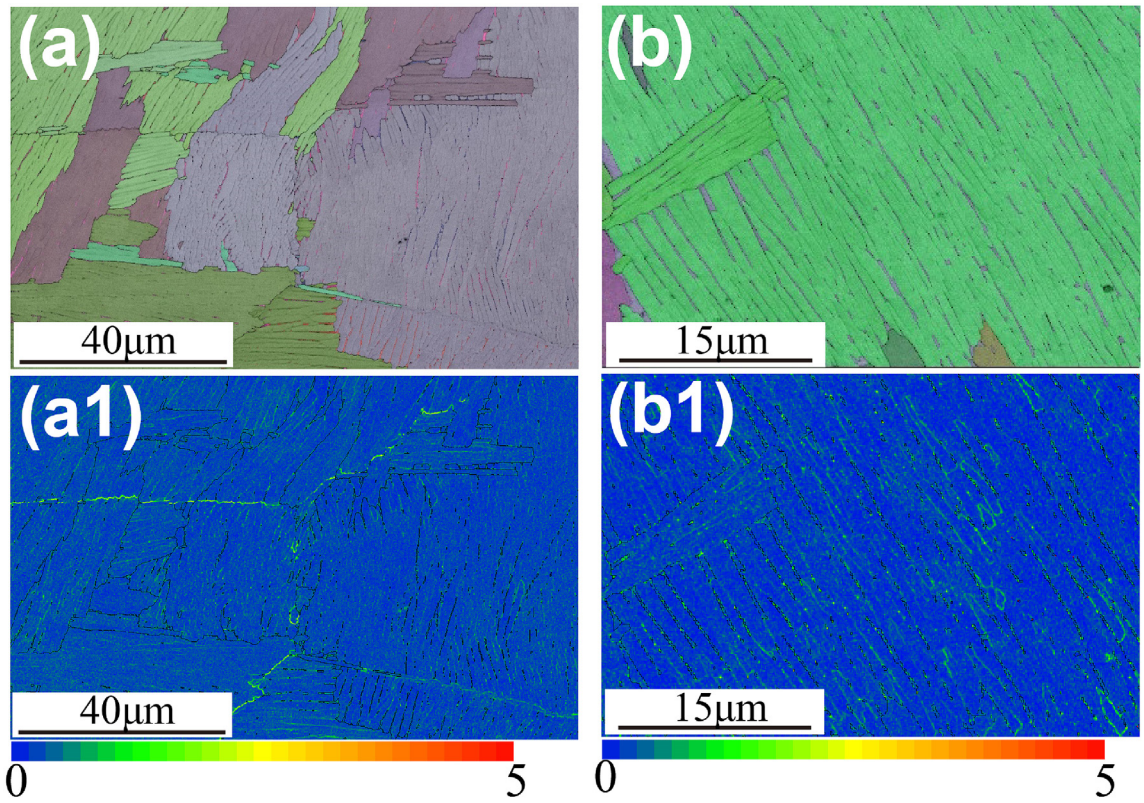

Fig. 11. Euler maps of (a) TC4 and (b) TC4F, and the corresponding local misorientation of (a1)TC4 and (b1)TC4F.

compositions of β phase are highlighted in solid blue squares. The phase boundary of β phase clearly indicates the increase of Fe content at the expense of decreased V. From the phase diagram, we understand that the almost identical chemical compositions of α in TC4 and TC4F, as well as the noticeable composition changes in β phase due to the trace addition of Fe, are the inevitable results governed by the phase equilibrium. As a strong β stabilizer, Fe triumphs over V in stabilizing β phase. The diluted V plus the micro-alloyed Fe are competent to maintain the β stability and to be equilibrium with the same α phase in TC4F. Since the solubility of V in α is limited, the diluted V in the β phase inevitably causes the increases in β phase fraction which is consistent with our SEM observation. It's worth noting that the values of element content show discrepancy between thermodynamic calculation and experiment, illustrated by the different β phase boundaries in Fig. 10. The dashed line in grey indicates the composition of β phase quenched from 712 °C, while the solid line in red is the equilibrium β phase boundary. The experimental compositions show smaller V and Fe contents than equilibrium values. The discrepancy might be attributed to two reasons: 1) 2 h annealing in the experiment is not long enough to allow a full element partitioning between α and β phases; 2) EPMA cannot accurately capture the content of element

Table 4
Chemical compositions of α and β phases in TC4 and TC4F alloys.

Alloy	Phase		Composition (at. %)			
	Phase	Location/State	Al	V	Fe	O
TC4	α	equilibrium	10.727	2.462	0.012	0.532
		matrix (away from tip)	10.325 ± 0.046	2.175 ± 0.053	0.015 ± 0.004	
		near crack tip	10.225 ± 0.053	2.135 ± 0.043	0.014 ± 0.003	
	β	equilibrium	8.484	15.667	1.561	0.055
		matrix (away from tip)	4.855 ± 0.104	13.265 ± 0.350	0.560 ± 0.018	
		near crack	4.835 ± 0.0.094	13.135 ± 0.390	0.556 ± 0.020	
TC4-F	α	equilibrium	10.862	2.195	0.023	0.427
		matrix (away from tip)	10.395 ± 0.094	2.260 ± 0.121	0.020 ± 0.016	
		near crack	10.267 ± 0.130	2.123 ± 0.014	0.023 ± 0.012	
	β	equilibrium	8.313	13.036	2.996	0.036
		matrix (away from tip)	6.074 ± 0.163	8.480 ± 0.156	1.140 ± 0.047	
		near crack	5.650 ± 0.055	10.232 ± 0.192	2.000 ± 0.048	

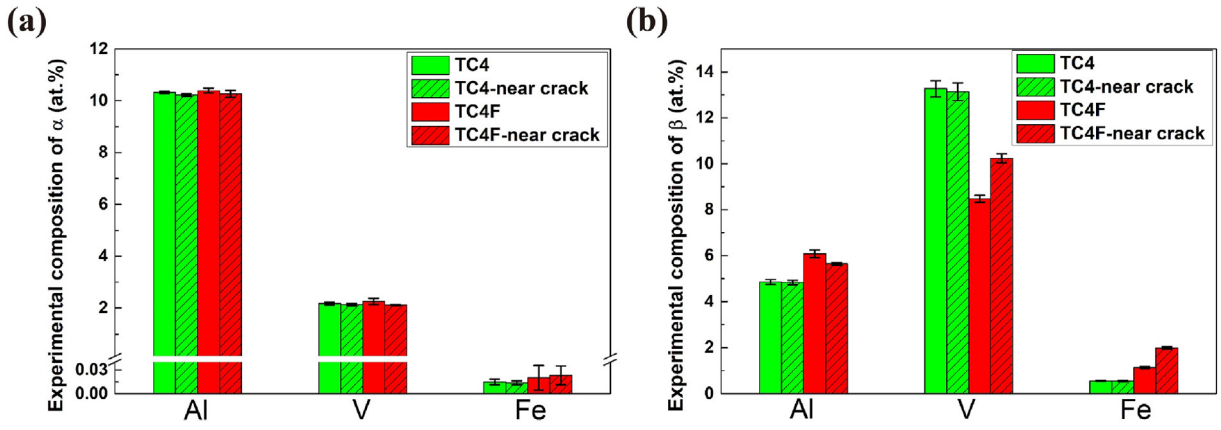

Fig. 12. The EPMA detected chemical compositions of α (a) and β (b) phases in TC4 and TC4F in different areas.

O in α and β, such that the contents of the remaining metallic elements may deviate. Despite the discrepancy, the composition change between V and Fe in the β phase is conclusive and considered the most apparent feature caused by the micro-alloying of Fe in TC4F. Fig. 14 presents the calculated equilibrium compositions of α and β phases in both alloys between 400 and 980 °C. The element contents in α of TC4 change with temperature, and the composition curves of individual elements almost coincide with those of TC4F. Whereas, noticeable differences in Fe and V contents in the β phase are found between TC4 and TC4F in the entire temperature range. It indicates the composition competition between Fe and V in β phase is universal in Ti-Al-V-Fe-O system, being valid not only at 712 °C but in the entire temperature range. Fe is known to be enriched in β phase and this enrichment may strengthen the β phase and do beneficial to enhance the interphase cohesion between β and α lamellae, thus suppresses interphase fracture.

Furthermore, TC4 and TC4F show different behaviors on local chemical compositions of β phase (Fig. 12). In the β phase of TC4, the chemical composition near the crack tip was measured identical to that in matrix away from the crack. Whereas the β phase in TC4F presents different local chemical compositions near and far away from the crack tip. It was measured Ti−5.65Al−10.23V−2.00Fe (at. %) near the crack tip, having V and Fe contents higher than those in the uncracked region. The crack propagation seems liable to take place in which combines more Fe and less dilute V. It means the Fe element can't be added indefinitely. The combination of few Fe and high V content in TC4 only exhibits a mediocre performance of fracture toughness, while the combination of high Fe and V contents in TC4F crack tip shows a higher sensitivity to crack propagation than TC4F matrix with less Fe and V. It is to assume that only a well-proportioned V and Fe in the β phase might help to increase the fracture toughness when the composition of the α phase was fixed. Other cases would lead to a deteriorated crack resistance.

3.7. Fracture toughness linked to Young's modulus

Based on the above characterizations, we discover that the trace addition of Fe has led to a noticeable decrease of V content and increase of Fe content in β phase together with a moderate increase of Young's modulus of alloy. Although the composition dependent Young's modulus of β phase in TC4 and TC4F is too narrow to be separately tested by using nanoindentation, the theoretical first principles calculations support the conclusion that the Fe alloying helps to enhance the phase stability, lattice vibration and modulus of β phase as well as alloy [34]. According to lattice dynamics, a nonlocal vibration mode of acoustic lattice wave can be associated with the combination of the strains [35]. The alloying of Fe contributes greater than other β stabilizers on lattice distortion and volume contraction in β phase [36]. The strains due to lattice distortion may have ability to trigger/suppress certain vibration modes and increase the Young's and bulk moduli of β phase, thereby affect elasticity, plasticity and even toughness [37].

Hahn and Rosenfield [38] proposed an empirical equation which expresses the plane strain fracture toughness parameter K_{IC} as the function of modulus, yield strength and fracture strain. It has been widely applied to reveal the mechanisms of fracture toughness in a

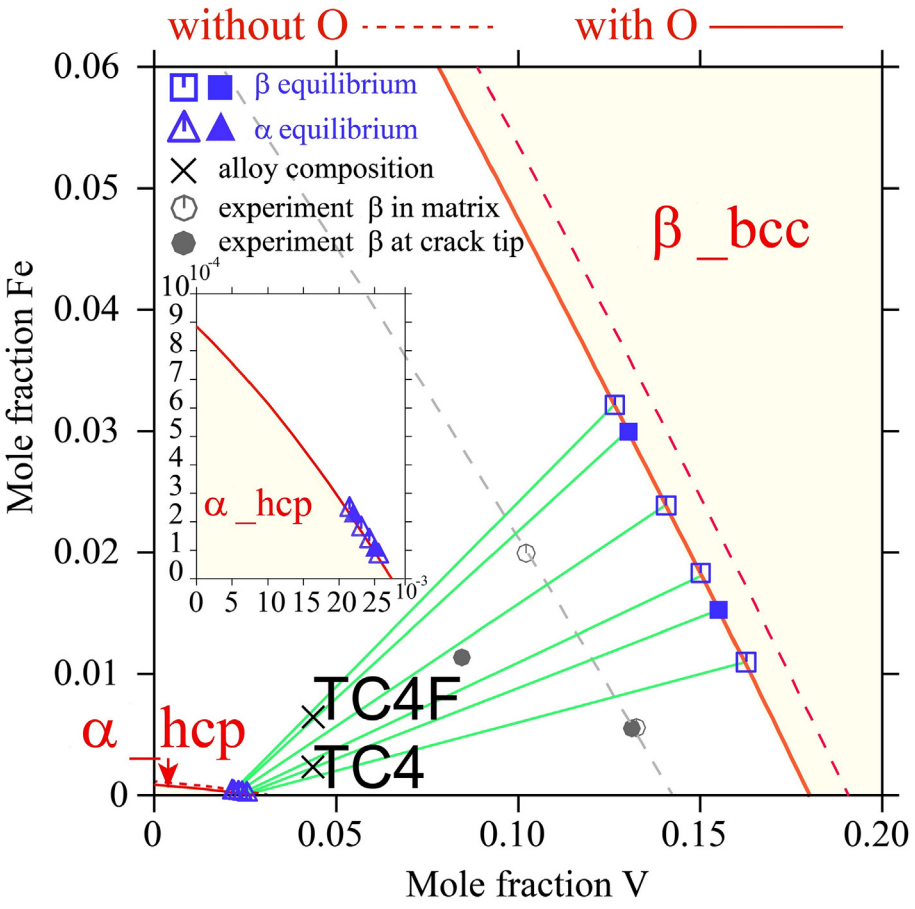

Fig. 13. The calculated 712°C isothermal phase boundaries with the independent variables of V and Fe mole fractions. The solid lines in red are equilibrium phase boundaries with O, while the dashed lines in red are without O. The equilibrium compositions of α and β phases are marked in triangles and squares. The black crosses, solid triangles and squares correspond to the compositions of alloys, equilibrium α and equilibrium β in TC4 and TC4F. The dashed line in grey indicates the composition of β phase quenched from 712 °C.

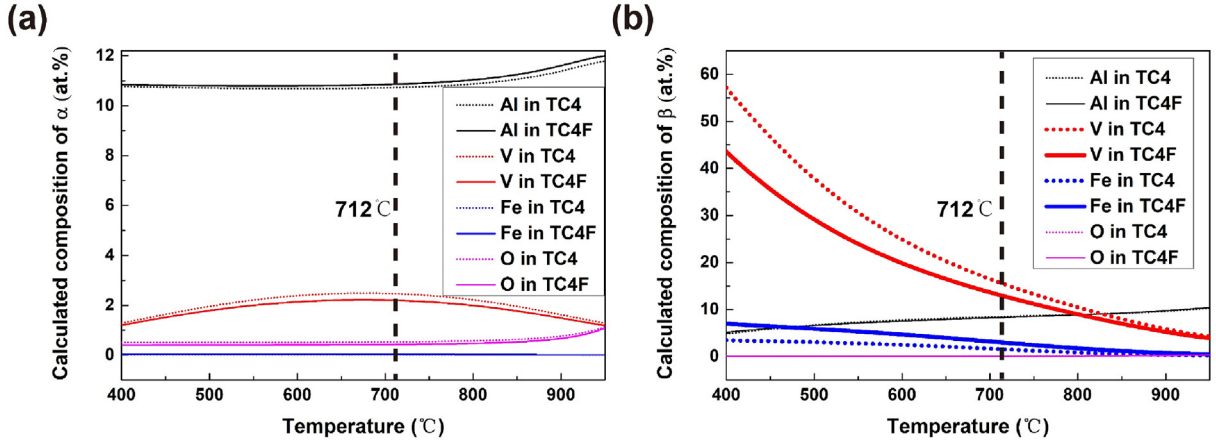

Fig. 14. The variations of calculated chemical compositions with temperatures in (a) α and (b) β.

variety of aluminum, and steel alloys [39,40].

$$K_{IC} = n\sqrt{cE\sigma_y\varepsilon_f} \quad (1)$$

where n is the strain hardening coefficient, σ_y the yield strength, ε_f fracture strain, E Young's modulus, and c is a constant depending on the state of stress. In this work, the fracture toughness K_{IC} of both TC4 and TC4F are predicted by using *Eq.* (1) and the mechanical properties of n, σ_y, E, ε in our tensile test (shown in Table 2). In particular, ε_f is taken as 1/3 of the final tensile elongation δ (suggested by Hahn and Rosenfield [38]). With a single adjustable parameter $c = 0.25$, the fracture toughness is predicted 87.93 MPa $m^{1/2}$ for TC4 and 114.81 MPa $m^{1/2}$ for TC4F which reproduce the measured fracture toughness well in Table 2 and Fig. 2. Among the independent variables in *Eq.* (1), only Young's

modulus reveals the intrinsic property of the alloy and can be written as the functions of V and Fe contents in thermodynamics. The good performance in fitting verifies the intrinsic connections among fracture toughness, Young's modulus, and chemical compositions. The rationality is inferred that the trace addition of Fe introduces the composition competition between V and Fe in the β phase, enhance Young's modulus and increase the fracture toughness of the alloy.

3.8. Limitations

In this work, only the chemical contributions to the fracture toughness in Fe modified TC4 is investigated. BASCA heat treatment basically eliminates the residual strain/stress in the deformed alloys, the preceding VAR and rolling have little effects on the microstructure observed and the mechanical properties tested. There is no extra driving force works in the heat treatment introduced β→α phase transformation besides the intrinsic thermodynamic contributions. The variation of microstructure features and mechanical properties, particularly the modulus and the fracture toughness can be mainly attributed to the effect of microalloying of Fe. The conclusions obtained from experiments and rationalization are fully based on the thermodynamics of alloys.

More than Young's modulus E, the fracture toughness is relevant to yield strength σ_y, fracture strain ε_f and work hardening n from *Eq.* (1) and also connected to the crack opening displacement. The latter category of properties are multi-value functionals of local stress/strain in the plastic zone ahead of the crack tip and influenced by the history of thermal-mechanical processing [41]. For β+α lamellar microstructure in this work, σ_y hardly changes with Fe addition vis-a-vis the enhancement in toughness due to the approximate stress-free state. The variation of modulus and microstructure feature with the addition of Fe is viewed as the major factor contributing to the increase in toughness, neglecting the local ductility at the crack tip. It is not true for TC4 with bimodal microstructure. The inhomogeneous distribution Fe coupled with local stress/strain retained from thermomechanical processing dramatically influences σ_y, ε_f, dislocation density as well as crack opening displacement, thus leads to a complex correlation between K_{IC} and all these parameters, which will be investigated further in separate papers.

4. Conclusions

In summary, the damage tolerance Ti−6Al−4V−0.55Fe alloy has been designed and fabricated through the micro-alloying of Fe to Ti−6Al−4V. The effect of trace addition of Fe on the microstructure developed and the mechanical properties have been investigated via combining experimental characterizations and thermodynamic calculations. The main discoveries are concluded below:

1. The trace Fe modified Ti−6Al−4V alloy exhibits remarkably improved fracture toughness, slightly increased hardness and elongation without significant reduction in yield strength and ultimate strength. The comprehensive mechanical property of TC4F has been proven better than prototype TC4, indicating the potential applications in industry.
2. The fracture toughness of heat treated TC4F with β+α lamellar microstructure matches the optimum grade of fracture toughness in TC4ELI and is demonstrated superior in comparison with that of TC4DT with various types of microstructure. It provides an effective and cost-reducing method to improve fracture toughness without precise control of interstitial elements.
3. The composition competition takes place between V and Fe in the β phase when Fe is added. It alters size and proportion characteristics of α and β phase. The occurrence of these behaviors has been validated and verified by experimental and thermodynamic calculation.
4. The mechanism of enhanced fracture toughness in TC4F is deduced to the complex composition competition between Fe and V. With the help Hahn-Rosenfield equation, the enhanced fracture toughness is correlated to the increased Young's modulus due to this composition redistribution.
5. The kinked β+α lamella is found nearby the crack of TC4F in contrast with bent α lamella in TC4. The intensified deformation enlarges the plastic zone ahead of crack tip propagation, changes direction of crack propagation and additionally contributes to the improvement of fracture toughness.

Data availability

The raw/processed data required to reproduce these findings cannot be shared at this time as the data also forms part of an ongoing study.

CRediT authorship contribution statement

Fuwen Chen: Methodology, Investigation, Validation, Formal analysis, Resources, Writing - original draft, Visualization, Funding acquisition. **Yulei Gu:** Investigation, Data curation. **Guanglong Xu:** Methodology, Validation, Formal analysis, Writing - review & editing, Visualization, Project administration, Funding acquisition. **Yuwen Cui:** Data curation, Writing - review & editing, Supervision, Funding acquisition. **Hui Chang:** Conceptualization, Resources, Supervision, Funding acquisition. **Lian Zhou:** Conceptualization, Supervision.

Acknowledgements

This work was supported by National Natural Science Foundation of China [Grants Nos. 51801101, 51701094, and 51602148], China Postdoctoral Science Foundation [Grant No. 2019M651812]. YC is acknowledged to the financial support from National Defense Basic Scientific Research Program of China [Grant No. JCKY2018414C020]. GX is acknowledged to the financial support from Natural Science Foundation of Jiangsu Province, China [Grant No. BK20171014]. The authors are thankful to Prof. Chuanhai Jiang at Shanghai Jiaotong University for the residual stress measurement.

Appendix A. Supplementary data

Supplementary data to this article can be found online at https://doi.org/10.1016/j.matdes.2019.108251.

References

[1] G. Lütjering, J.C. Williams, Titanium, Springer Science & Business Media, 2007.
[2] R.R. Boyer, Titanium for aerospace: rationale and applications, Adv. Perform. Mater. 2 (1995) 349−368.
[3] R.R. Boyer, An overview on the use of titanium in the aerospace industry, Mater. Sci. Eng. A 213 (1996) 103−114.
[4] C. Cui, B.M. Hu, L. Zhao, S. Liu, Titanium alloy production technology, market prospects and industry development, Mater. Des. 32 (2011) 1684−1691.
[5] X. Tan, Y. Kok, Y.J. Tan, M. Descoins, D. Mangelinck, S.B. Tor, K.F. Leong, C.K. Chua, Graded microstructure and mechanical properties of additive manufactured Ti−6Al−4V via electron beam melting, Acta Mater. 97 (2015) 1−16.
[6] X. Zhao, S. Li, M. Zhang, Y. Liu, T.B. Sercombe, S. Wang, Y. Hao, R. Yang, L.E. Murr, Comparison of the microstructures and mechanical properties of Ti−6Al−4V fabricated by selective laser melting and electron beam melting, Mater. Des. 95 (2016) 21−31.

[7] W.S.W. Harun, N.S. Manam, M.S.I.N. Kamariah, S. Sharif, A.H. Zulkifly, I. Ahmad, H. Miura, A review of powdered additive manufacturing techniques for Ti-6Al-4V biomedical applications, Powder Technol. 331 (2018) 74–97.
[8] G. Shen, D. Furrer, Manufacturing of aerospace forgings, J. Mater. Process. Technol. 98 (2000) 189–195.
[9] C. Liu, D. Liu, X. Zhang, Dan Liu, A. Ma, N. Ao, X. Xu, Improving fatigue performance of Ti-6Al-4V alloy via ultrasonic surface rolling process, J. Mater. Sci. Technol. 35 (2019) 1555–1562.
[10] P. Barriobero-Vila, G. Requena, T. Buslaps, M. Alfeld, U. Boesenberg, Role of element partitioning on the α–β phase transformation kinetics of a bi-modal Ti–6Al–6V–2Sn alloy during continuous heating, J. Alloy. Comp. 626 (2015) 330–339.
[11] P. Barriobero-Vila, G. Requena, T. Buslaps, G.A. Hartman, Dual fatigue failure modes in Ti–6Al–2Sn–4Zr–6Mo and consequences on probabilistic life prediction, Scr. Mater. 48 (2003) 1637–1642.
[12] J.V. Scanlan, G.J.G. Chambers, Forgings in Titanium alloys//The Science, Technology and Application of Titanium: Proceedings of an International Conference Organized by the Institute of Metals, the Metallurgical Society of Aime, and the American Society for Metals in Association with the Japan Institute of Metals and the Academy of Sciences, USSR, and Held at Th, Elsevier, 2013, pp. 79–96.
[13] S. Sandlöbes, S. Korte-Kerzel, D. Raabe, On the influence of the heat treatment on microstructure formation and mechanical properties of near-α Ti-Fe alloys, Mater. Sci. Eng. A 748 (2019) 301–312.
[14] M.L. Meier, D.R. Lesuer, A.K. Mukherjee, The effects of the α/β phase proportion on the superplasticity of Ti-6Al-4V and iron-modified Ti-6Al-4V, Mater. Sci. Eng. A 154 (1992) 165–173.
[15] M.J. Bermingham, S.D. McDonald, D.H. StJohn, M.S. Dargusch, Segregation and grain refinement in cast titanium alloys, J. Mater. Res. 24 (2009) 1529–1535.
[16] A. Ogawa, M. Niikura, C. Ouchi, K. Minikawa, M. Yamada, Development and applications of titanium alloy SP-700 with high formability, J. Test. Eval. 24 (1996) 100–109.
[17] R.C. Alderliesten, Designing for damage tolerance in aerospace: a hybrid material technology, Mater. Des. 66 (2015) 421–428.
[18] S. Sadeghpour, S.M. Abbasi, M. Morakabati, S. Bruschi, Correlation between alpha phase morphology and tensile properties of a new beta titanium alloy, Mater. Des. 121 (2017) 24–35.
[19] G. Welsch, R. Boyer, E.W. Collings, Materials Properties Handbook: Titanium Alloys, ASM international, 1993.
[20] M. Seifi, M. Dahar, R. Aman, O. Harrysson, J. Beuth, J.J. Lewandowski, Evaluation of orientation dependence of fracture toughness and fatigue crack propagation behavior of as-deposited ARCAM EBM Ti-6Al-4V, JOM 67 (2015) 597–607.
[21] ASM 4907 D, Titanium Alloy, Sheet, Strip, and Plate, 6.0Al-4.0V, Extra Low Interstitial, Annealed, SAE International. AMS G Titanium and Refractory Metals Committee, 1965.
[22] Y. Ma, D. Wang, H. Wang, J. Lei, J. Wang, Y. Liu, Q. Gao, R. Yang, Factors influencing fracture toughness of TC4ELI alloy, Chin. J. Nonferrous Metals 20 (2010) 414–418.
[23] P. Guo, Y. Zhao, W. Zeng, Q. Hong, The effect of microstructure on the mechanical properties of TC4-DT titanium alloys, Mater. Sci. Eng. A 563 (2013) 106–111.
[24] X. Zhu, H. Chang, Y. Xie, L. Ding, H. Li, Y. Cui, L. Zhou, Hot deformation behavior of two kinds of TC4-xfe alloys based on processing map, Rare Metal Mater. Eng. 46 (2017) 204–210.
[25] Y. Fan, J. Cao, H. Yang, Z. Chen, L. Li, Effect of Fe content on mechanical properties of Ti-6Al-4V alloy, Heat Treat. Met. 38 (2013) 21–23.
[26] ASTM E8/E8M–09, Standard Test Methods for Tension Testing of Metallic Materials, ASTM International, Pennsylvania (United States), 2009.
[27] ASTM E399-06, Standard Test Method for Linear-Elastic Plane-Strain Toughness KIC of Metallic Materials, ASTM International, Pennsylvania (United States), 2006.
[28] N. Dumontet, D. Connétable, B. Malard, B. Viguier, Elastic properties of the α'martensitic phase in the Ti-6Al-4V alloy obtained by additive manufacturing, Scr. Mater. 167 (2019) 115–119.
[29] J.K. Fan, J.S. Li, H.C. Kou, K. Hua, B. Tang, The interrelationship of fracture toughness and microstructure in a new near β titanium alloy Ti–7Mo–3Nb–3Cr–3Al, Mater. Char. 96 (2014) 93–99.
[30] I. Sen, S. Tamirisakandala, D.B. Miracle, U. Ramamurty, Microstructural effects on the mechanical behavior of B-modified Ti–6Al–4V alloys, Acta Mater. 55 (2007) 4983–4993.
[31] B.R. Sridhar, G. Devananda, K. Ramachandra, R. Bhat, Effect of machining parameters and heat treatment on the residual stress distribution in titanium alloy IMI-834, J. Mater. Process. Technol. 139 (2003) 628–634.
[32] J.A. Sutliff, An investigation of plastic strain in copper by automated-EBSP, Microsc. Microanal. 2 (1999) 236–237.
[33] L.N. Brewer, M.A. Othon, L.M. Young, T.M. Angeliu, Misorientation mapping for visualization of plastic deformation via electron back-scattered diffraction, Microsc. Microanal. 12 (2006) 85–91.
[34] W. Zhou, R. Sahara, K. Tsuchiya, First-principles study of the phase stability and elastic properties of Ti-X alloys (X= Mo, Nb, Al, Sn, Zr, Fe, Co, and O), J. Alloy. Comp. 727 (2017) 579–595.
[35] R.A. Cowley, Acoustic phonon instabilities and structural phase transitions, Phys. Rev. B 13 (1976) 4877.
[36] L.F. Huang, B. Grabowski, J. Zhang, M.J. Lai, C.C. Tasan, S. Sandlöbes, J. Neugebauer, From electronic structure to phase diagrams: a bottom-up approach to understand the stability of titanium–transition metal alloys, Acta Mater. 113 (2016) 311–319.
[37] N.V. Skripnyak, A.V. Ponomareva, M.P. Belov, I.A. Abrikosov, Ab initio calculations of elastic properties of alloys with mechanical instability: application to BCC Ti-V alloys, Mater. Des. 140 (2018) 357–365.
[38] G.T. Hahn, A.R. Rosenfield, Sources of Fracture Toughness: the Relation between K_{Ic} and the Ordinary Tensile Properties of metals//Applications Related Phenomena in Titanium Alloys, ASTM International, 1968.
[39] G.T. Hahn, A.R. Rosenfield, Metallurgical factors affecting fracture toughness of aluminum alloys, Metall. Trans. A 6 (1975) 653–668.
[40] G.T. Hahn, A.R. Rosenfield, Local yielding and extension of a crack under plane stress, Acta Metall. 13 (1965) 293–306.
[41] G. Lütjering, Influence of processing on microstructure and mechanical properties of (α+ β) titanium alloys, Mater. Sci. Eng. A 243 (1998) 32–45.